Tracking sulfate, magnesium and amorphous phases in Rosalina-like benthic foraminifera

Guillaume Paris[1], Caroline Thaler[2,3,*], Marc Dellinger[4], Jérôme Aléon[5], Smail Mostefaoui[5], Alice Aléon-Toppani[6], Claire Rollion-Bard[3], David Troadec[7], Guillaume Yangshu Wang[8], Annachiara Bartolini[2]

[1] Université de Lorraine, CNRS, CRPG, F-54000 Nancy, France

[2] Centre de Recherche en Paléontologie -Paris (CR2P), MNHN, CNRS, Sorbonne Université, F-75005 Paris, France

[3] Laboratoire des Sciences du Climat et de l'Environnement (LSCE), UMR 8212 CEA, CNRS, Université de Versailles Saint-Quentin en Yvelines, F-91191 Gif sur Yvette Cedex

[4] MCAM, UMR 7245 MNHN, CNRS, Sorbonne Université, 75005 Paris, France

[5] Institut de Minéralogie, de Physique des Matériaux et de Cosmochimie (IMPMC), Sorbonne Université, MNHN, CNRS UMR 7590, IRD, F-75005 Paris, France

[6] Université Paris-Saclay, CNRS, Institut d'Astrophysique Spatiale, F-91405 Orsay, France

[7] Université de Lille, CNRS, Centrale Lille, Junia, Université Polytechnique Hauts de France, UMR 8520-IEMN, F-59000 Lille, France

[8]Université Paris Cité, Laboratoire Matériaux et Phénomènes Quantiques UMR 7162, 75205 Paris, France

* Now at Ecobloom

Supplementary material

Description of *Rosalina* sp.

The test is plano-convex in shape, with a trochospiral pattern, and is rather compressed. The spiral side is in fact gently convex and the umbilical side is slightly concave. All the rapidly enlarging chambers are clearly visible on the convex spiral side, particularly under an optical microscope, the sutures are depressed and oblique, curving back at the periphery. On the umbilical side, the chambers appear subtriangular due to the presence of an acuminate extremity named 'flap' or 'folium', which extends over the umbilical region. The sutures are slightly curved. The interior of the chambers is simple and undivided. The periphery is subacute with no keel present. The aperture is a low interior marginal arch bordered by a lip and located near the periphery on the umbilical side. It is separated from a small secondary opening by the umbilical folium. The test is hyaline calcitic with a smooth, perforated surface.

However, there are certain differences compared to the type species of the genus, *Rosalina globularis,* d'Orbigny, 1826. These differences can be attributed to the morphological variability within this genus. These include a more evolute spiral coiling in the final whorl, which results in less overlap of the chambers on the umbilical side, and an ovoid rather than circular outline. Furthermore, significant morphological occurs within the For1C1 strain, with two distinct morphotypes (Thaler et al., 2023). Individuals of the first morphotype reproduce asexually every 12–15 days once their test has developed 11–12 chambers and morphologically resemble the Rosalina genus. Contrastingly, the others survive for several weeks and develop over 12 chambers, with those in the final whorl tending to become more elongated and arranged in a more irregular fashion. Both morphotypes of the For1C1 strain are attached to the substratum. High morphological variability is typical of attached forms, even more so in larger specimens (more than 12 chambers). Reproducing individuals of the For1C1 strain are likely to be diploid macrospheric schizonts that have entered an apogamic cycle of successive asexual reproduction (Thaler et al. 2023). During this cycle, the new generation of schizonts is produced by schizogony (i.e. the multiple fission of a multinucleate parental cytoplasm). Therefore, as already discussed in Thaler et al. 2023, it is difficult to identify them morphologically at the species level because the morphology of the diploid microspheric agamont and/or the haploid macrospheric gamont parent generation, on which species descriptions are often based, is, to the best of our knowledge, unknown. Indeed, the morphology of the macrospheric diploid schizont, macrospheric haploid gamont, and microspheric diploid agamont generations can differ considerably. For this reason, we will use the species-level identification open and use the designation *Rosalina* sp.

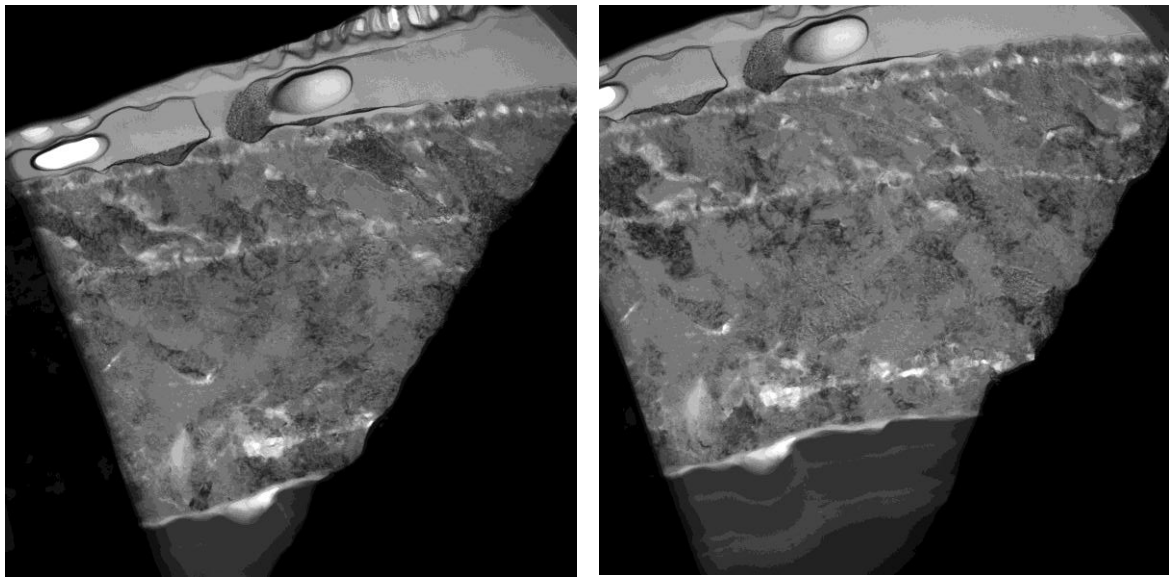


Figure S1 TEM bright field views with -5° (left panel) and 0° (right panel) tilting angles showing how the white lines remain white regardless of the inclination, as well as shifting levels of gray for the OCLs

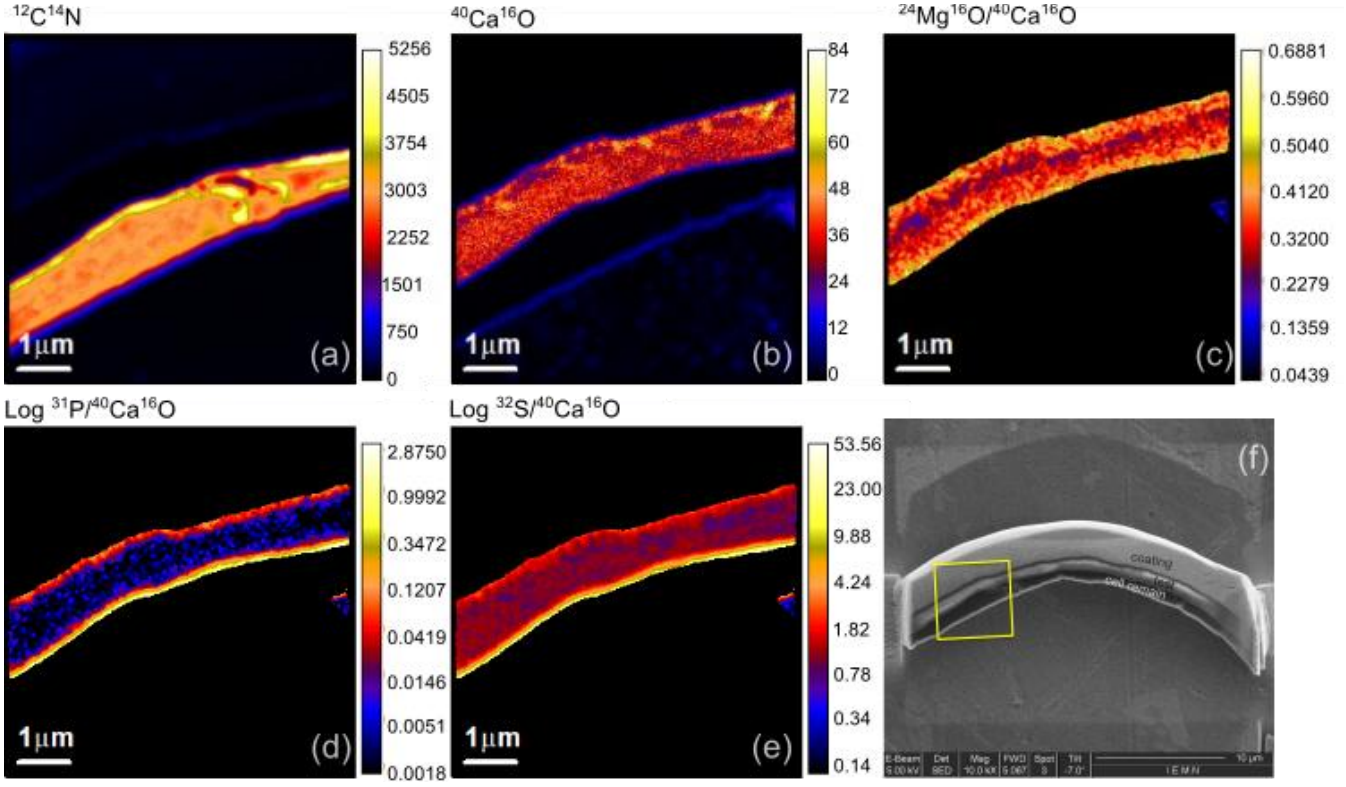


Figure S2. $^{12}C^{14}N$, $^{40}Ca^{16}O$, $^{24}Mg^{16}O/^{40}Ca^{16}O$, $^{32}S/^{40}Ca^{16}O$ and $^{31}P/^{40}Ca^{16}O$, maps in foraminifera *Pseudorosalina* Banyuls (For1C1), previous to last chamber (A1n-1, Image 20)

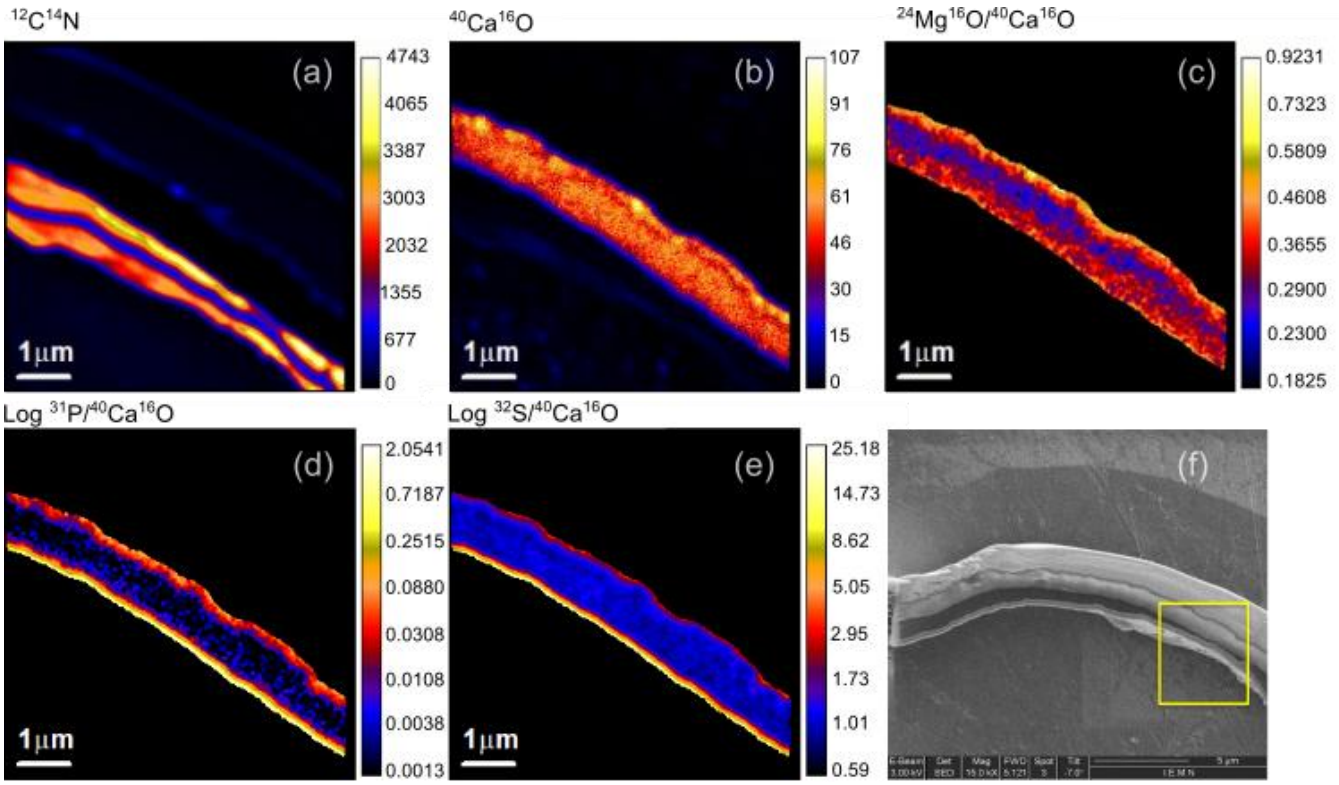


Figure S3. $^{12}C^{14}N$, $^{40}Ca^{16}O$, $^{24}Mg^{16}O/^{40}Ca^{16}O$, $^{32}S/^{40}Ca^{16}O$ and $^{31}P/^{40}Ca^{16}O$ maps in foraminifera *Pseudorosalina* Banyuls (For1C1) A1, last chamber (A1n, Image 21)

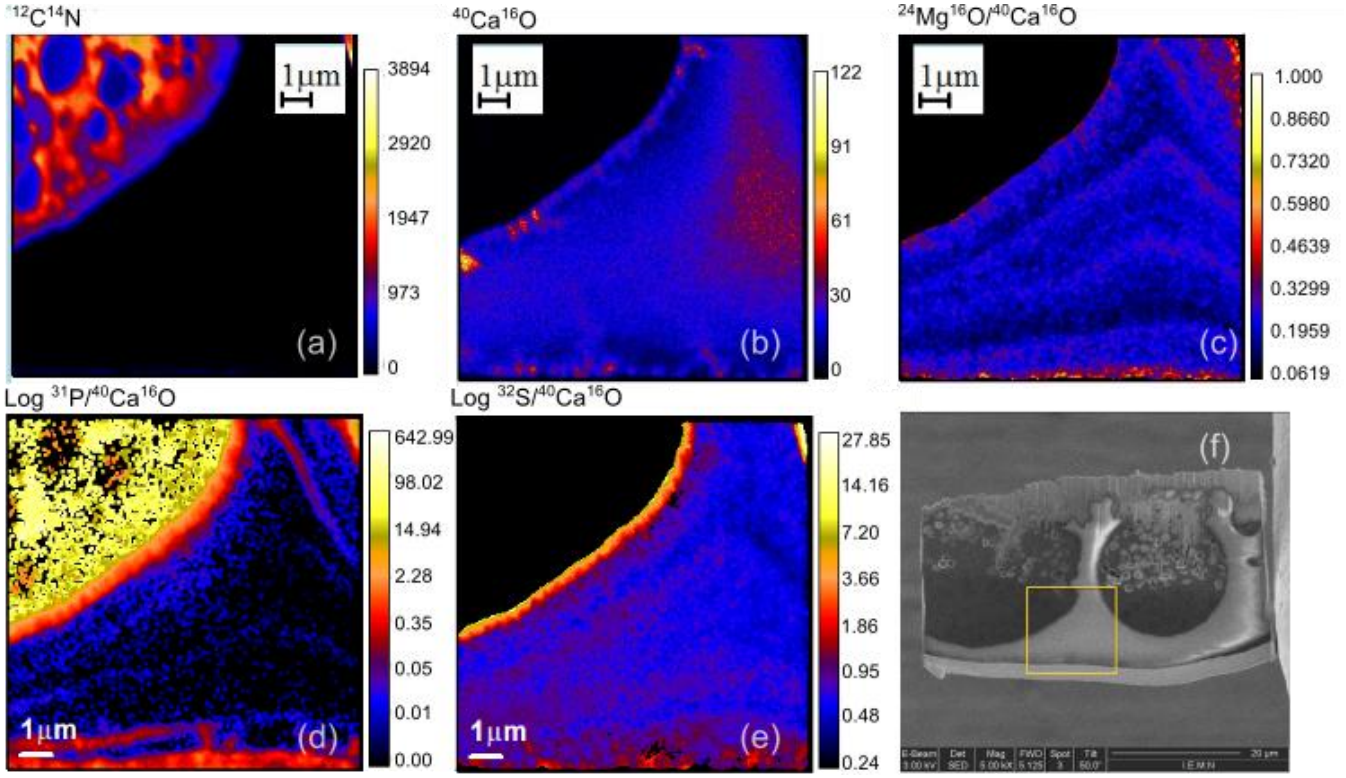


Figure S4 $^{12}C^{14}N$, $^{40}Ca^{16}O$, $^{24}Ca^{16}O/^{40}Ca^{16}O$, $^{32}S^{40}Ca^{16}O$ and $^{31}P/^{140}Ca^{16}O$ maps across the FIB section of foraminifera F5(2)B3 (culture in doubled sulfate concentration seawater), chambers n-3 and n-5/6. Mg, S and P are represented only in the test (mask applied over the cytoplasm)

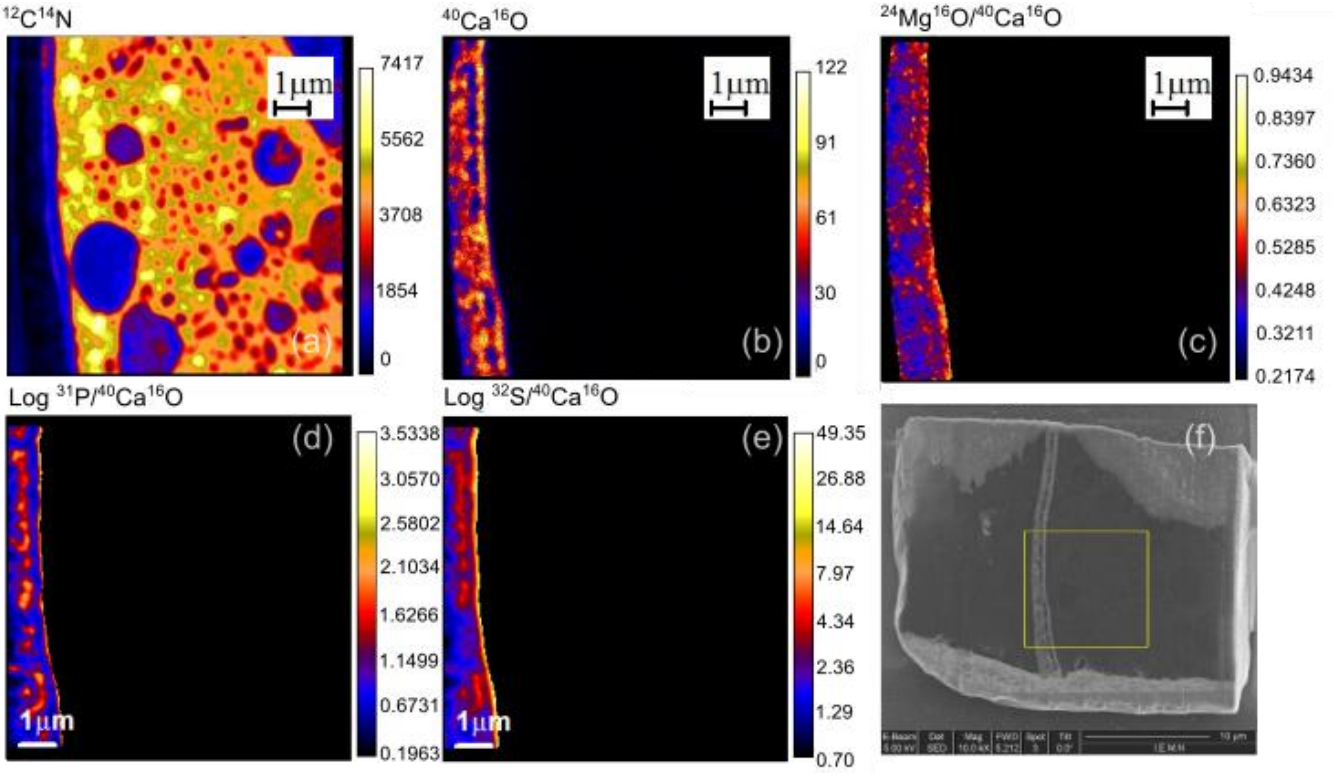


Figure S5 $^{12}C^{14}N$, $^{40}Ca^{16}O$, $^{24}Ca^{16}O/^{40}Ca^{16}O$, $^{32}S^{40}Ca^{16}O$ and $^{31}P/^{140}Ca^{16}O$ maps across the FIB section of foraminifera F2A2 chamber n. Mg, S are represented only in the test (mask applied over the cytoplasm).

90

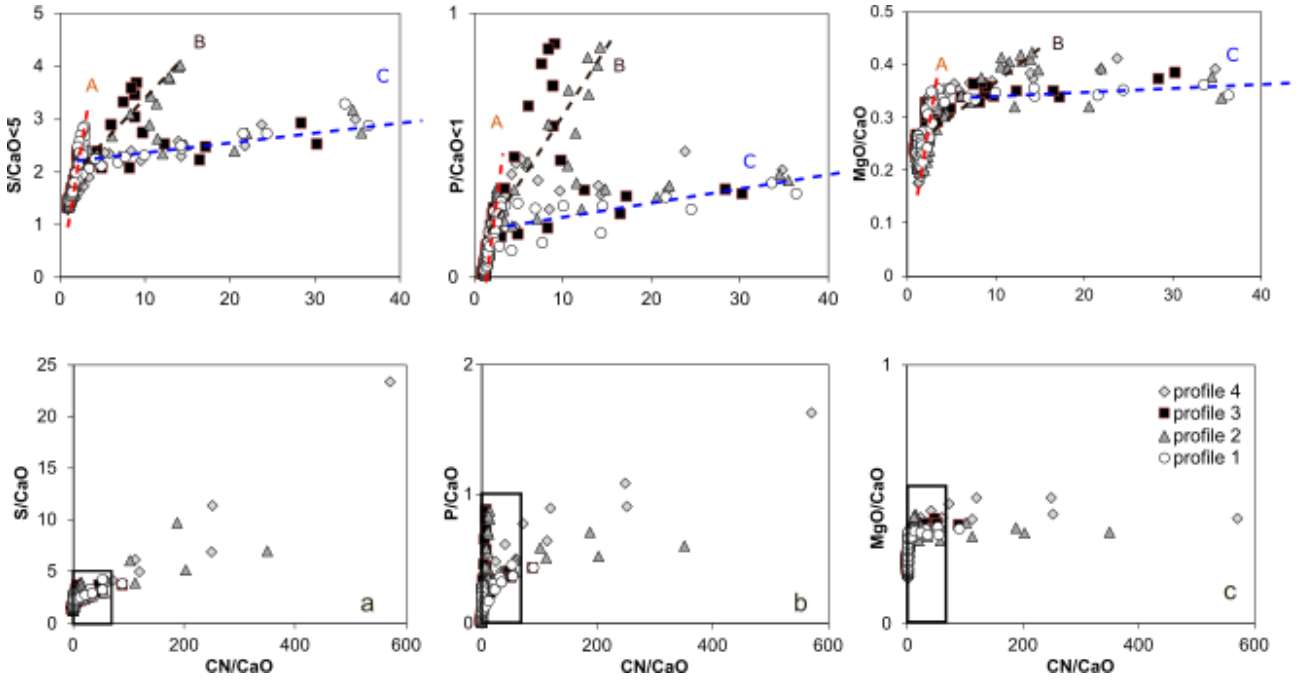


Figure S6 Cross plots of elemental distribution across the test combining 4 profiles across the F5(2)B1 section, with three indicative trends, corresponding to the full dataset used for figure 4 in the main text. The data are coded by profile and not trend, unlike Fig. 4.

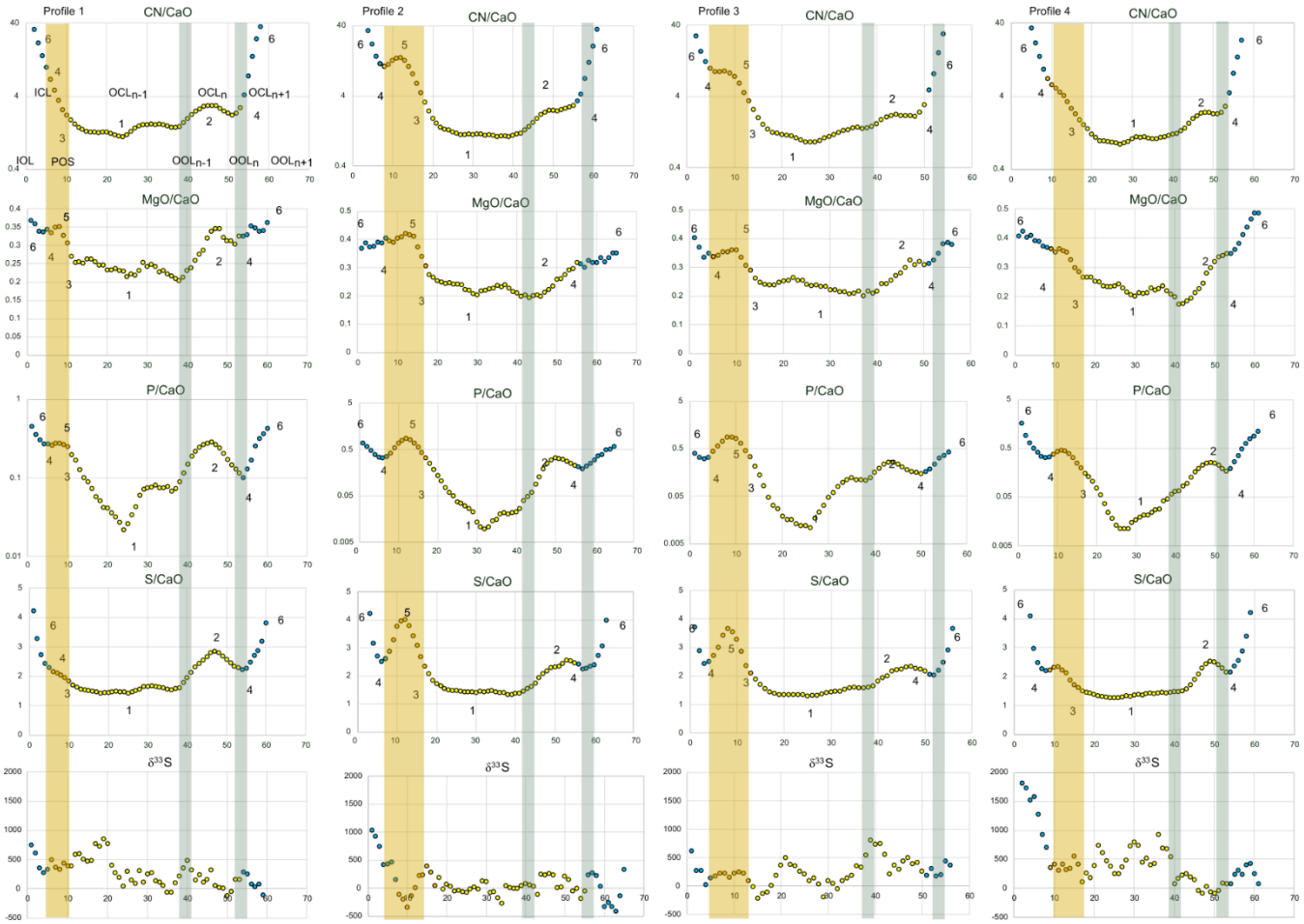


Figure S7 Element ratio distributions across for the 4 individual profiles performed across the FIB section F5(2)B1. The orange bars corresponds to points distributed along trend B, the grey bars correspond the OOL as observe in the HAADF TEM views. Digits represent the different endmembers of trends A, B and C, also indicated in Fig. 4.